Crack Detection and Dynamic Analysis of a Cracked Rotor with Soft Bearings Using Different Methods of Solution

Lucas Rangel de Oliveira(✉) and Gilberto Pechoto de Melo(✉)

Universidade Estadual Paulista, Ilha Solteira, SP 15385-000, Brazil
{lucas.r.oliveira, gilberto.pechoto}@unesp.br

Abstract. The ratio of bearing stiffness to the shaft stiffness has a significant impact on the lower frequencies, mode shapes and, consequently, the whirl orbits. Most works studying crack detection methods in rotating systems use bearings relatively stiff, where the shaft bending is very pronounced. This paper analyzes how the nonlinear effect of the crack in the whirl orbits and the diagnostic forces technique for detecting cracks behave for soft bearings. The results show that the extra loops, very well known in the literature, are not present for the soft bearings. On the other hand, diagnostic peaks were successful in both cases. The efficiency of these methods depends on the mathematical model of the cracked rotor. This work considers the breathing mechanism in formulating the time-varying finite element stiffness matrix of the cracked element, requiring the solution of a set of equations at each time-step. With this concern, two approaches for the solution of the dynamic response are compared: direct time integration method using Newmark's method and solution of discrete-time state equations. The Newmark's method requires small time-step for the accuracy of the response, however, the processing time is much smaller when compared to solution of discrete-time state equations.

Keywords: Rotating machines · Crack identification · Multiple scales method
Discrete-time state equation · Newmark method

1 Introduction

Large fluctuations of internal tension may cause transverse cracks in the shaft due to the intense demand in a rotating system. During the operation of a flexible shaft, the weight itself produces a bending that induce the crack to open and close repeatedly. This condition causes the stiffness at that location to be synchronized with the angle of rotation. This mechanism is called "breathing crack".

Several papers were published on the theoretical and experimental study of the dynamic analysis and the development of methodologies for detection and diagnosis of cracked shaft [1–4], in addition to extensive literature reviews showing the particularity of each model and condensing the information presented over the years [5–7].

The first step in understanding its dynamic effects is to find an effective model of breathing crack. Davies and Mayes [8] describe a method for calculating the rotor response supported by multiple bearings and relate the change in stiffness of the shaft to

K. L. Cavalca and H. I. Weber (Eds.): IFToMM 2018, MMS 61, pp. 3–17, 2019.
https://doi.org/10.1007/978-3-319-99268-6_1

its depth. The passage from the opening to the total closing of the crack is considered smooth, with a harmonic characteristic dependent on the angular position of the rotor. In a simpler modeling of the crack breathing – in which it considers only two states: totally open and totally closed – Gasch [9] analyzes the dynamic behavior and the stability of transverse cracked rotor.

In more current papers, the crack effect is considered by the time-varying area moment of inertia of the cross-sectional area of the cracked element together with the function that represents the crack breathing effect. Sinou and Lees [10] analyze the changes in the natural frequency of the rotor for different crack depths and the dynamic behavior of the rotor close to 1/2x of the resonant frequency. To calculate the response of the cracked rotor, the authors use the harmonic balance method, which allows to discretize functions unknown in time using its Fourier components. The influence of crack is provided by the change of moments of inertia according to the crack depth and the breathing effect are represented by a sinusoidal function presented by Davies and Mayes [8].

In 2011, Al-Shudeifat and Butcher [1] presented two new functions – one for each axis of coordinates – to represent the crack breathing effect and proposes new equations to calculate the variation of the area moments of inertia of the cross section of the cracked element. The paper carried out a comparison with the modeling used in [10]. The results were promising: the moments of inertia of the new model correctly corresponded with reality and the new breathing functions presented more accurate results for the dynamic behavior of the cracked rotor.

The motivation of several studies to identify crack signatures in their early stages is to support in the early crack detection before damage occurs because of its propagation. Mani et al. [11] proposes to use Active Magnetic Bearings (AMBs) to apply known dynamic forces at certain frequencies generating a combinational resonance – through the multiple scale method – aiming to evidence characteristic crack signatures in the spectral responses. In this paper, the author uses the crack model of Gasch.

Sawicki et al. [12] uses the above technique, however, with the Mayes crack modeling and compares experimental and analytical analysis. In the same year, Sawicki et al. [13] proposed to replace the multiple scales method with an approximation based on the harmonic balance method to estimate the combinational resonances and to validate this method experimentally.

Recently, Cavalini et al. [2] used the technique of diagnostic forces applied at certain frequencies by the multiple scales method together with a pseudo-random optimization code known as Differential Evolution (DE) to characterize the crack signatures in the spectral responses of the rotor. Two crack models are considered: ‘open crack’ and ‘breathing crack’ model. Although the diagnostic technique has proved to be efficient, the crack breathing models used in previous paper are not as accurate as the model proposed in Al-Shudeifat and Butcher [1].

In the literature, the studies about crack detection methods use systems where stiffness bearings coefficients are stiffer than the shaft stiffness, called “stiff bearing”. However, the system behavior is greatly changed (including the orbits) in systems where stiffness bearings coefficients is low relative to shaft stiffness, called “soft bearings”.

This paper analyzes how two of the main crack detection methods – the appearance of extra loops in whirl orbits in subcritical speeds and diagnostics peaks on the spectral responses – behave for the soft bearings.

This work considers the breathing mechanism in formulating the time-varying finite element stiffness matrix of the cracked element, requiring the solution of a set of equations at each time-step. With this concern, two approaches for the solution of the dynamic response are compared: direct time integration method using Newmark's method and solution of discrete-time state equations. This comparison considers the accuracy of the system response and the ratio between the processing time of each method.

2 Crack Modeling

The calculation for the moment of inertia of the crack element presented in [1] produced more accurate results when compared to models used in works of [10, 14–16]. Here, this model is employed and reviewed briefly.

The crack is modeled as shown in Fig. 1a, where the dashed segment represents the crack segment. As the shaft begins to rotate, the crack angle with the negative Y axis is changed by time to Ωt, as shown in Fig. 1b [1, 17, 18].

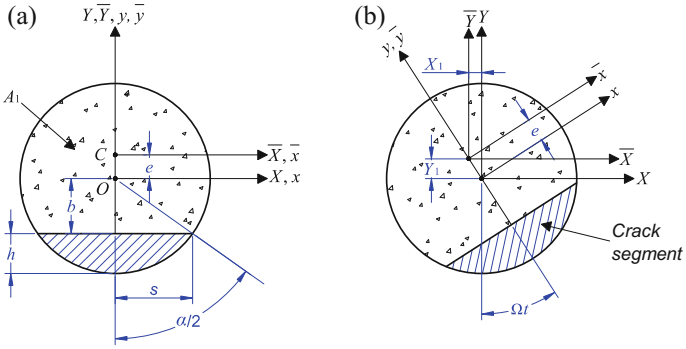

Fig. 1. Coordinate system for the cracked rotor.

The cross-sectional area A_1 of the crack element and the location of the centroid e on the fixed Y axis at $t = 0$ are given by

$$A_1 = R^2\left[\pi - \cos^{-1}(1-\mu) + (1-\mu)\gamma\right] \tag{1}$$

$$e = \frac{2R^3}{3A_1}\gamma^3 \tag{2}$$

$$\gamma = \sqrt{\mu(2-\mu)} \tag{3}$$

where h is the crack depth, R is the radius of the crack element and $\mu = h/R$ the non-dimensional crack depth, as shown in Fig. 1.

The coordinate systems used in calculating the positions of the centroid and the neutral axis of the cracked element are changed instantly during the rotation of the shaft. From Fig. 2, the upper end of the crack edge reaches the compression stress field at angle θ_1, which means that the crack begins to close at that angle. At angle θ_2, the crack is completely closed. These two important angles are given by

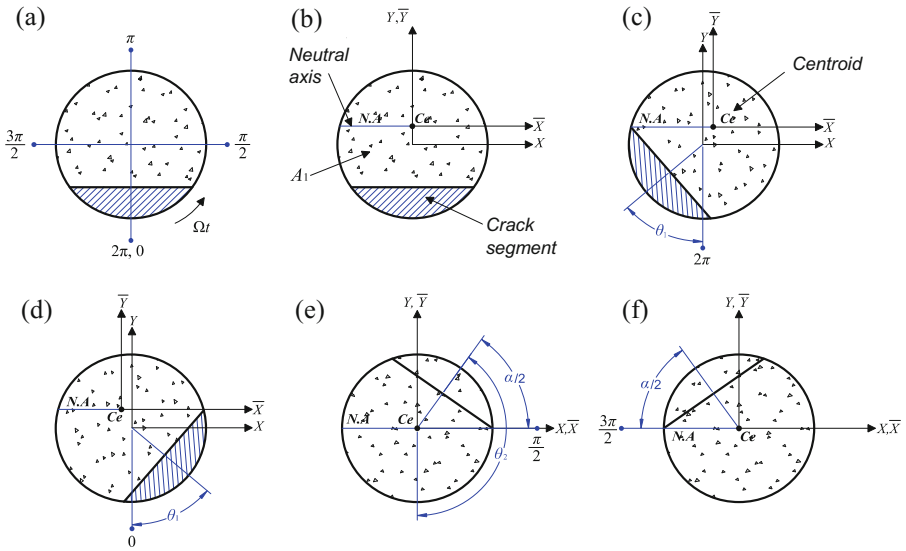

Fig. 2. Crack breathing condition and centroid location of the cross section of the cracked element at different angles of rotation.

$$\theta_1 = \tan^{-1}\left[\frac{e + R(1-\mu)}{R\sqrt{\mu(2-\mu)}}\right] \tag{4}$$

$$\theta_2 = \frac{\pi}{2} + \cos^{-1}(1-\mu) \tag{5}$$

The crack states for full angle rotate can be divided into three regions: fully open in the interval $2\pi - \theta_1 \leq \Omega t < \theta_1$ (Fig. 2c–d); fully closed in the interval $(\pi + \alpha)/2 \leq \Omega t < (3\pi - \alpha)/2$ (Fig. 2e–f); partially open in the intervals $\theta_1 \leq \Omega t < (\pi + \alpha)/2$ or $(3\pi - \alpha)/2 \leq \Omega t < 2\pi - \theta_1$.

The area moments of inertia of A_1 on the rotated x and y axes for $t \leq 0$ are denoted by I_1 and I_2, respectively, and are calculated by

$$I_1 = I - I_x^c \tag{6}$$

$$I_2 = I - I_y^c \tag{7}$$

where I is the area moment of inertia of the shaft cross-section for the fully closed crack ($I = \pi R^4/4$), and I_x^c e I_y^c the area moments of inertia of the crack segment on the rotated x and y axes for t $\leq$ 0, given by

$$I_x^c = \frac{\pi R^4}{8} - \frac{R^4}{4}\left[(1-\mu)\left(2\mu^2 - 4\mu + 1\right)\gamma + \sin^{-1}(1-\mu)\right] \tag{8}$$

$$I_y^c = \frac{\pi R^4}{12}\left[(1-\mu)\left(2\mu^2 - 4\mu - 3\right)\gamma + 3\sin^{-1}(\gamma)\right] \tag{9}$$

The area moments of inertia of A_1 about the centroidal rotated $\bar{x}$ and $\bar{y}$ axes for t $\geq$ 0 are calculated by

$$\bar{I}_1 = I_1 - A_1 e^2 \tag{10}$$

$$\bar{I}_2 = I_2 \tag{11}$$

According to [19], the area moments of inertia of A_1 on the fixed axes X and Y are time-varying according to the shaft rotation and can be expressed in terms of I_1 and I_2 by

$$I_X^{A_1}(t) = \frac{I_1 + I_2}{2} + \frac{I_1 - I_2}{2}\cos(2\Omega t) + I_{12}\sin(2\Omega t) \tag{12}$$

$$I_Y^{A_1}(t) = \frac{I_1 + I_2}{2} + \frac{I_1 - I_2}{2}\cos(2\Omega t) - I_{12}\sin(2\Omega t) \tag{13}$$

Considering the cross section of the crack element symmetric about y axis, the term $I_{12} = 0$. At angle that the crack starts to close, the closed portion of the crack, A_2, is a time-varying quantity. Thus, the overall cross-section area of the crack element is given by

$$A_{ce}(t) = A_1 + A_2(t) \tag{14}$$

Thus, the area moments of inertia of the crack element about the X and Y axes are given by

$$I_X(t) = I_X^{A_1}(t) + I_X^{A_2}(t) \tag{15}$$

$$I_Y(t) = I_Y^{A_1}(t) + I_Y^{A_2}(t) \tag{16}$$

According to the parallel axes theorem, the area moment of inertia of $A_{ce}(t)$ about the $\bar{X}$ and $\bar{Y}$ axes which stay parallel to the fixed X and Y axes during the shaft rotation are given by

$$I_{\bar{X}}(t) = I_X(t) - Y_{ce}^2(t)A_{ce}(t) \tag{17}$$

$$I_{\bar{Y}}(t) = I_Y(t) - X_{ce}^2(t)A_{ce}(t) \tag{18}$$

where $X_{ce}(t)$ and $Y_{ce}(t)$ are the instantaneous centroids coordinates of the $A_{ce}(t)$ about the fixed X and Y axes. Calculations of the area, centroid and the area moments of inertia of the cracked element cross-section are described in [1], Appendix B. Equations (17) and (18) are time-varying and periodic, so can be approximated by Fourier series expansion, $\hat{I}_{\bar{X}}(t)$ and $\hat{I}_{\bar{Y}}(t)$. Rewriting them based on Eqs. (10) and (11)

$$I_{\bar{X}}(t) \cong \hat{I}_{\bar{X}}(t) = I - (I - \bar{I}_1)f_1(t) \tag{19}$$

$$I_{\bar{Y}}(t) = \hat{I}_{\bar{Y}}(t) = I + (I - \bar{I}_1)f_1(t) - (2I - \bar{I}_1 - \bar{I}_2)f_2(t) \tag{20}$$

$$f_1(t) = \cos^n(\Omega t/2) \tag{21}$$

$$f_2(t) = \frac{1}{\pi}\left[\frac{\theta_1 + \theta_2}{2} - \frac{2}{\theta_2 - \theta_1}\sum_{i=1}^{p}\frac{\cos(i\theta_2) - \cos(i\theta_1)}{i^2}\cos(i\Omega t)\right] \tag{22}$$

Considering $I_{11} = I - \bar{I}_1$ and $I_{22} = 2I - \bar{I}_1 - \bar{I}_2$, Eqs. (19) and (20) can be rewritten by [1]

$$\hat{I}_{\bar{X}}(t) = I - I_{11}f_1(t) \tag{23}$$

$$\hat{I}_{\bar{Y}}(t) = I + I_{11}f_1(t) - I_{22}f_2(t) \tag{24}$$

The finite element stiffness matrix of the cracked element by the Al-Shudeifat modeling is given by

$$\boldsymbol{k}^{crack} = \boldsymbol{k} + \boldsymbol{k}_1 f_1(t) + \boldsymbol{k}_2 f_2(t) \tag{25}$$

where $\boldsymbol{k}$ is the stiffness matrix of the fully-closed crack element which is equivalent to the stiffness element of the uncrack element [20, 21], $\boldsymbol{k}_1$ and $\boldsymbol{k}_2$ are the stiffness matrices which consider the area moment of inertia of the crack element due to the breathing crack described in [1].

3 Motion Equation of the Cracked Rotor

The rotor consists of a flexible horizontal shaft, two disks and two ball bearings supported by two springs that allow to regulate the stiffness of the bearings (Fig. 3a). The model discretization and the finite element is shown in Fig. 3b. The parameters and dimensions of the system are described in Table 1.

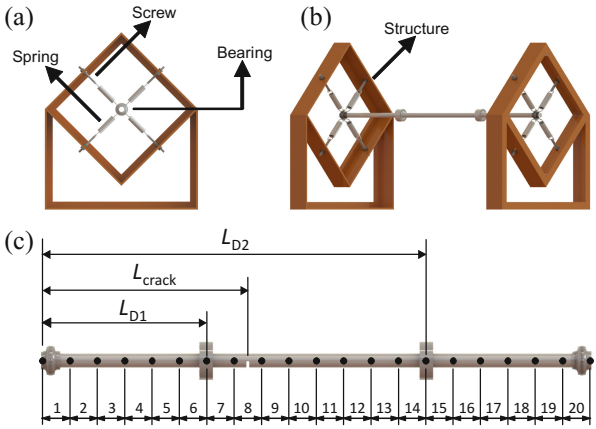

Fig. 3. Rotating system configuration with a structure that allows to change the bearings coefficients. (a) Front view. (b) Side view. (c) Finite element model of rotor-disk-bearing system.

Table 1. Physical parameters of the system.

Parameters	Values	Parameters	Values
Length of the shaft	1 m	Modulus of elasticity	$2.1\ 10^{11}$ N m^{-2}
Length of the finite element	0.05 m	Poisson ratio	0.3
Radius of the shaft	0.0075 m	Density of rotor	7800 kg m^{-3}
Position of the disk 1 (L_{D1})	0.3 m	Unbalance	$2\ 10^{-4}$ m kg
Position of the disk 2 (L_{D2})	0.7 m	Soft bearing stiffness	$5\ 10^{3}$ N m^{-1}
Outer diameter of the disks	0.040 m	Stiff bearing stiffness	$5\ 10^{6}$ N m^{-1}
Inner diameter of the disks	0.015 m	Bearing damping	100 Ns m^{-1}
Thickness of the disks	0.015 m	Coefficient of damping	10^{-5}

The shaft is discretized into twenty beam elements. Each node has four degrees of freedom, consisting of two translational and rotational displacement about the X and Y axis, described by the nodal displacement vector $\vec{q}_i(t) = \{u_i\, v_i\, \theta_i\, \psi_i\}^T$ to $i = 1, 2, \ldots, 21$.

Each rigid disk is discretized into just one node – with the same degrees of freedom of the shaft. The bearings are considered support elements represented by stiffness coefficients and damping coefficients [20, 21].

The assembly of the element matrices ensures that each of the element matrix rows and columns (mass, stiffness and damping) is identified by the corresponding degree of freedom and placed in their appropriate locations in the overall matrix of the assembled system. After this procedure, the equation of motion is written by [10]

$$\boldsymbol{M}\ddot{\vec{q}}(t)+\boldsymbol{D}(t)\dot{\vec{q}}(t)+\boldsymbol{K}^{crack}(t)\vec{q}(t)=\vec{f}(t) \tag{26}$$

where $\vec{f}(t)$ is the forces vectors; $\boldsymbol{M}$ is the mass matrix of the shaft with the disk; $\boldsymbol{D}(t)$ includes the shaft's damping, the damping of the bearings and also the gyroscopic effect of the shaft with the disk; $\boldsymbol{K}^{crack}(t)$ represents the stiffness matrix of the shaft with the time-varying stiffness of the crack element. The vector $\vec{q}(t)=\{\vec{q}_1(t),\ldots,\vec{q}_N(t)\}^T$ includes the translational and rotational node displacements of the full system. The shaft's damping is taken as proportional to stiffness $\boldsymbol{D}_{shaf}=\eta\boldsymbol{K}_{shaft}$, where η is a constant factor of proportionality [10].

4 Solutions Methods

In 1959 Newmark presented an integration method to find the solution of a system based on the approximation of its acceleration vector, using the Taylor approach for the displacement and speed vectors [22, 23]. Approaching the vectors $\ddot{\vec{q}}(t)$, $\dot{\vec{q}}(t)$, $\vec{q}(t)$ and $\vec{f}(t)$ by $\ddot{\vec{q}}_n$, $\dot{\vec{q}}_n$, $\vec{q}_n$ and $\vec{f}_n$ at $t=n\tau$ with a positive time-step $\tau=t_{n+1}-t_n$ and an integer n, Eq. (26) can be written by

$$\boldsymbol{M}\ddot{\vec{q}}_{n+1}+\boldsymbol{D}_{n+1}\dot{\vec{q}}_{n+1}+\boldsymbol{K}^{crack}_{n+1}\vec{q}_{n+1}=\vec{f}_{n+1} \tag{27}$$

The Newmark family of time integration algorithms requires the displacement and velocity to be updated as [24]

$$\begin{aligned}\vec{q}_{n+1}&=\vec{q}_n+\tau\dot{\vec{q}}_n+1/2\tau^2\ddot{\vec{q}}_n+\beta\tau^2\left(\ddot{\vec{q}}_{n+1}-\ddot{\vec{q}}_n\right)\\ \dot{\vec{q}}_{n+1}&=\dot{\vec{q}}_n+\tau\ddot{\vec{q}}_n+\gamma\tau\left(\ddot{\vec{q}}_{n+1}-\ddot{\vec{q}}_n\right)\end{aligned} \tag{28}$$

where β and γ are Newmark's integration parameters.

Based on Eq. (28), Newmark's method generates the approximation sequence by the following iteration steps given by [24]

$$\begin{aligned}\ddot{\vec{q}}_0&=\boldsymbol{M}^{-1}\left(\vec{f}_0-\boldsymbol{D}_0\dot{\vec{q}}_0-\boldsymbol{K}^{crack}_0\vec{q}_0\right)\\ \ddot{\vec{q}}_{n+1}&=\left(\boldsymbol{M}+\gamma\tau\boldsymbol{D}_n+\beta\tau^2\boldsymbol{K}^{crack}_n\right)^{-1}\Big[-\boldsymbol{K}^{crack}_n\vec{q}_n-\left(\boldsymbol{D}_n+\tau\boldsymbol{K}^{crack}_n\right)\dot{\vec{q}}_n+\\ &\quad\left\{(\gamma-1)\tau\boldsymbol{D}_n+(\beta-1/2)\tau^2\boldsymbol{K}^{crack}_n\right\}\ddot{\vec{q}}_n+\vec{f}_{n+1}\Big]\end{aligned} \tag{29}$$

In order to obtain a state-space representation, Eq. (26) can take the following form

$$\begin{aligned}\dot{\vec{x}}(t) &= \boldsymbol{A}(t)\vec{x}(t) + \boldsymbol{B}\vec{u}(t)\\ \vec{y}(t) &= \boldsymbol{C}\vec{x}(t)\end{aligned} \tag{30}$$

where

$$\boldsymbol{A}(t) = \begin{bmatrix} \boldsymbol{0} & \boldsymbol{I} \\ -\boldsymbol{M}^{-1}\boldsymbol{K}^{crack}(t) & -\boldsymbol{M}^{-1}\boldsymbol{D}(t) \end{bmatrix}; \boldsymbol{B} = \begin{bmatrix} \boldsymbol{0} \\ \boldsymbol{M}^{-1} \end{bmatrix}; \boldsymbol{C} = [\boldsymbol{C}_{oq} \quad \boldsymbol{C}_{ov}]; \vec{x}(t) = \begin{Bmatrix} \vec{q}(t) \\ \dot{\vec{q}}(t) \end{Bmatrix}$$

where $\vec{x}(t)$ is the state vector, $\vec{y}(t)$ is the output vector, $\vec{u}(t)$ is the input vector, $\boldsymbol{C}_{oq}$ and $\boldsymbol{C}_{ov}$ are the output displacement and velocity matrices (defined by the variables of interest), $\boldsymbol{I}$ is the identity matrix and $\boldsymbol{0}$ is the null matrix.

The state is the information that must be stored and updated at the simulation. Thus, given the initial state vector, input vector, and physical parameters of the system, it is possible to find the state vector as well the output vector by a recursive formula by using first-order difference equations [25]

$$\begin{aligned}\vec{x}_{n+1} &= \boldsymbol{A}_n^d\vec{x}_n + \boldsymbol{B}^d\vec{u}_n\\ \vec{y}_n &= \boldsymbol{C}^d\vec{x}_n\end{aligned} \tag{31}$$

where $\boldsymbol{A}^d, \boldsymbol{B}^d, \boldsymbol{C}^d$ are the discrete matrices of the Eq. (30) for the sampling time τ.

5 Dynamic Analysis and Crack Detection Methodology

The critical speeds and modes shapes depend on the magnitude of the bearing stiffness, bearing position and the mass and stiffness of the rotor. More specifically, the ratio of bearing stiffness to the shaft stiffness has a significant impact on the critical speeds, mode-shapes and, consequently, the whirl orbits [26].

According to the ratio of bearing stiffness to the shaft stiffness, the rotor can be classified into three versions: soft, intermediate and stiff bearings. For the soft bearings, the bearing stiffness is low relative to the shaft stiffness, the natural frequencies are controlled by the bearing stiffness and the shaft almost no bending. Conversely, for stiff bearing, the bearings are much stiffer than the shaft, the lower natural frequencies are controlled by the shaft stiffness and increase bearing stiffness would not change the natural frequencies. For intermediate bearing, both contribute to the modal behavior of the system [20, 26]. The bearing stiffness diagram, Fig. 4, summarizes the three versions. The gray arrow indicates the bearing stiffness coefficients used.

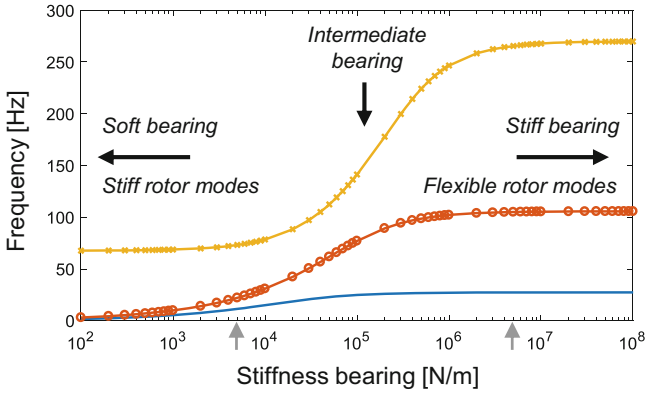

Fig. 4. Frequency versus stiffness bearing (two gray arrows indicate the bearing stiffness values used).

As well-known in the literature, the continuous variation of the stiffness in rotating coordinate system influences the frequency composition, generating higher frequency components in the response (2×, 3×, …), unlike for the uncracked rotor where the dynamic response is purely synchronous (without harmonics).

The effect of these components on the rotor orbits is visualized by the appearance of extra loops through subcritical speeds (1/2×, 1/3×, …). It is important to emphasize that the behavior of the orbits during passage through the subcritical forward whirl is different from that at the subcritical backward whirl. As well shown in [1], the change in the phase and amplitude of the response causes the appearance of outer loops during the passage through the subcritical backward whirl and inner loops during the passage through the subcritical forward whirl.

The analysis of the crack effect is visualized during the passage through subcritical forward whirl of the right bearing for two cases: soft bearing (k_{soft} = 5 kN/m) and stiff bearing (k_{stiff} = 5 MN/m), considering an unbalance mass located at the left disk. In the system with stiff bearing, the inner loop formed due to dominant second harmonic component indicating is clearly seen. As the crack depth increases, the amplitude of the harmonic component becomes more significant and the inner loop get larger, as shown in Fig. 5a to c. These effects are like those found in the literature.

However, for the soft bearing the influence of the crack was not significant in the system response, which can be explained due to the change in system behavior, since the shaft not bend very much, and its mode shape is like a rigid rotor. This behavior can be visualized even at greater depths crack, as shown in Fig. 5d to f.

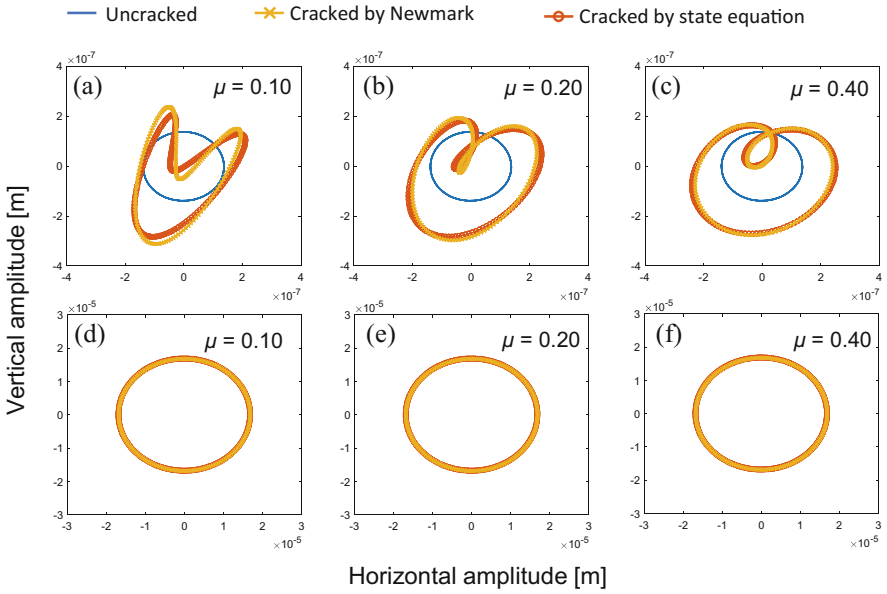

Fig. 5. Whirl orbits of the right bearing during passage through 1/2 of critical whirl speed for different crack depth for the stiff bearings (a-c) and soft bearings (d-f).

In order to investigate the influence of the time-step on the solution methods, the sampling rate was obtained by dividing the number of samples, N_d, per time required for one revolution of the shaft. Thus, the higher the N_d the lower the time-step resulting in a more accurate solution. This analysis was performed for two depth cracks, only for the stiff bearing, since in the other case there was no loop formation and the response of the cracked and uncracked rotor was the same. The effect of time-step in the solution methods is shown in Fig. 6 by comparing the appearance of the inner loop in whirl orbits of the cracked rotor.

The solution by the Newmark method requires a smaller time-step so that the response is not incorrectly calculated. However, the final simulation time was considerably smaller (about fifty times faster) compared to the solution by discrete-time state equation. It was verified that the highest computational cost of this last method was due to the discretization of matrices $\boldsymbol{A}$, $\boldsymbol{B}$, $\boldsymbol{C}$ of the state equation, Eq. (30), to be inserted in Eq. (31).

The influence of the crack is not significant in the soft bearing response, as shown in Fig. 5. However, there is a method which success have been theoretically and experimentally proven in many studies. In this technique, forces are applied to the system to induce the rotor to combination resonances [2, 13, 27–30]. These signatures are diagnostic peaks that arise due to the nonlinear effect in the rotor caused by the presence of crack.

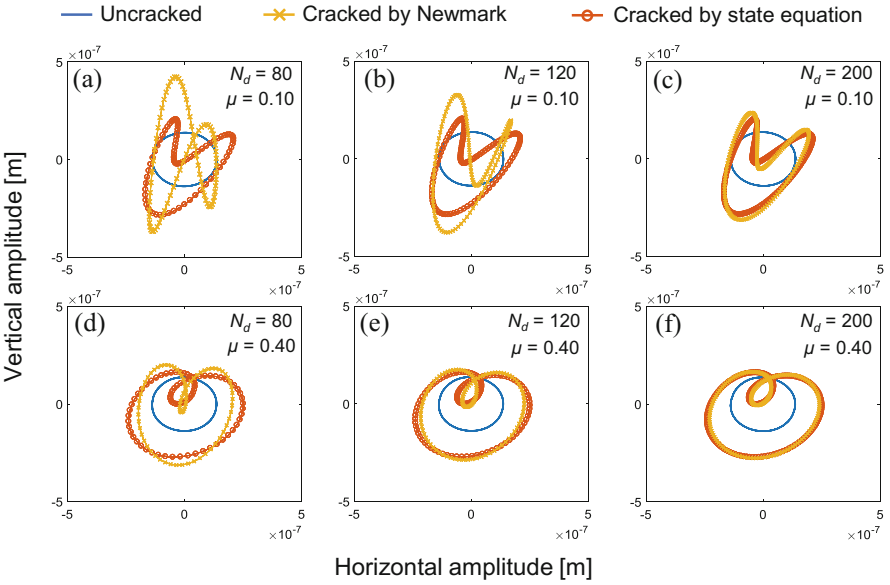

Fig. 6. Whirl orbits of the right bearing during passage through 1/2 of critical whirl speed for different time-step for the stiff bearings with depth crack $\mu = 0.10$ and $\mu = 0.40$.

According to [2, 11], the conditions required for a combination resonance occurs when

$$\Omega_{diag} = \left| k\,\Omega - \omega_{fw} \right|, \quad \text{to} \quad k = \pm 1, \pm 2, \pm 3, \ldots \tag{32}$$

where Ω is the rotation speed and ω_{fw} is critical speed (forward whirl) of the rotor.

Changing the values of the stiffness bearings coefficients modifies the modal properties of the system. Thus, the rotation speed, critical frequency and frequency of diagnostic forces used to induce the combination resonance in the system are described in Table 2. For the spectral response in Fig. 7 (obtained from the solution by discrete-time state equation) an amplitude of 50 N for the diagnostic forces was applied at the left bearing, both for stiff bearing, Fig. 7a-b, and soft bearing, Fig. 7c-d.

Table 2. Frequencies used in the combination resonances method.

	Rotation speed	Critical speed	Diagnostic frequency ($k = -1$)
Soft bearing	8 Hz	11.48 Hz	19.48 Hz
Stiff bearing	20 Hz	27.39 Hz	47.39 Hz

The use of diagnostic forces is able to show the peaks associated with the combination of resonances, harmonic component frequencies and critical frequencies for both soft bearing and stiff bearing. As expected, the increase in crack depth caused the

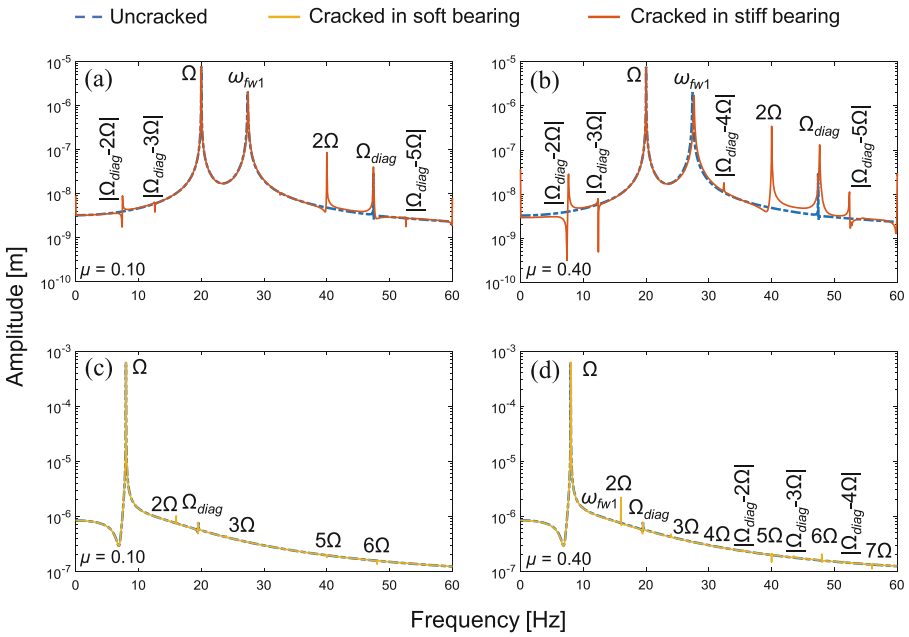

Fig. 7. Diagnostic peaks on the FFT response for right bearing position in vertical direction.

increase in resonance peaks because the nonlinear effect becomes more evident in the system responses. This relationship can be used as a tool to estimate the depth of the crack [2].

6 Conclusion

The analysis performed in this work investigates the nonlinear effect of crack in soft bearing systems, in which modal behavior at low frequencies are controlled by the stiffness coefficients of the bearings. A second analysis is how the solution method of the motion equations can affect the cracked rotor response.

As well known in the literature, the effect of the harmonic components was clearly seen by the appearance of inner loops in the whirl orbit of the cracked rotor for the stiff bearing system. However, the influence of the crack was not significant for the soft bearing system, where the uncracked and cracked rotor responses did not change.

The technique of crack detection by the application of diagnostic forces proved to be efficient when applied in both systems. The diagnostic peaks are smaller when compared to the stiff bearing system. However, even with smaller peaks for the system with stiff bearings, this technique is a promising tool to satisfactorily estimate the existence and depth of a transverse crack found in rotating machine shafts. In addition, the amplitude of the force can be adjusted to further evidence the peaks as long as it keeps a safe vibration level.

The time-step significantly impacts the solution of the dynamic response of cracked rotor. Newmark's method is very sensitive to time-step, requiring smaller values when compared to the discrete-time state equation. However, the computational efficiency of the Newmark method, measured by processing time, is considerably higher.

References

1. Al-Shudeifat, M.A., Butcher, E.A.: New breathing functions for the transverse breathing crack of the cracked rotor system: approach for critical and subcritical harmonic analysis. J. Sound Vib. **330**, 526–544 (2011)
2. Cavalini Jr., A.A., Sanches, L., Bachschmid, N., Steffen Jr., V.: Crack identification for rotating machines based on a nonlinear approach. Mech. Syst. Signal Process. **79**, 72–85 (2016)
3. Guo, C., Yan, J., Yang, W.: Crack detection for a Jeffcott rotor with a transverse crack: an experimental investigation. Mech. Syst. Signal Process. **83**, 260–271 (2017)
4. Bachschmid, N., Pennacchi, P., Tanzi, E.: A sensitivity analysis of vibrations in cracked turbogenerator units versus crack position and depth. Mech. Syst. Signal Process. **24**, 844–859 (2010)
5. Kan, M.S., Tan, A.C.C., Mathew, J.: A review on prognostic techniques for non-stationary and non-linear rotating systems. Mech. Syst. Signal Process. **62–63**, 1–20 (2015)
6. Papadopoulos, C.A.: The strain energy release approach for modeling cracks in rotors: a state of the art review. Mech. Syst. Signal Process. **22**, 763–789 (2008)
7. Sabnavis, G., Kirk, R.G., Kasarda, M., Quinn, D.: Cracked shaft detection and diagnostics: a literature review. Shock Vib. Dig. **36**, 287–296 (2004)
8. Davies, W.G.R., Mayes, I.W.: The vibrational behavior of a multi-shaft, multi-bearing system in the presence of a propagating transverse crack. J. Vib. Acoust. Stress Reliab. Des. **106**, 146–153 (1984)
9. Gasch, R.: A survey of the dynamic behaviour of a simple rotating shaft with a transverse crack. J. Sound Vib. **160**, 313–332 (1993)
10. Sinou, J.-J., Lees, A.W.: The influence of cracks in rotating shafts. J. Sound Vib. **285**, 1015–1037 (2005)
11. Mani, G., Quinn, D.D., Kasarda, M.: Active health monitoring in a rotating cracked shaft using active magnetic bearings as force actuators. J. Sound Vib. **294**, 454–465 (2006)
12. Kulesza, Z., Sawicki, J.T.: Auxiliary state variables for rotor crack detection. J. Vib. Control **17**, 857–872 (2011)
13. Sawicki, J.T., Friswell, M.I., Kulesza, Z., Wroblewski, A., Lekki, J.D.: Detecting cracked rotors using auxiliary harmonic excitation. J. Sound Vib. **330**, 1365–1381 (2011)
14. Sinou, J.-J.: Effects of a crack on the stability of a non-linear rotor system. Int. J. Non-Linear Mech. **42**, 959–972 (2007)
15. Sinou, J.-J.: Detection of cracks in rotor based on the $2\times$ and $3\times$ super-harmonic frequency components and the crack–unbalance interactions. Commun. Nonlinear Sci. Numer. Simul. **13**, 2024–2040 (2008)
16. Sinou, J.-J., Faverjon, B.: The vibration signature of chordal cracks in a rotor system including uncertainties. J. Sound Vib. **331**, 138–154 (2012)
17. Shudeifat, M.A.: Stability analysis and backward whirl investigation of cracked rotors with time-varying stiffness. J. Sound Vib. **348**, 365–380 (2015)

18. Guo, C., AL-Shudeifat, M.A., Yan, J., Bergman, L.A., McFarland, D.M., Butcher, E.A.: Application of empirical mode decomposition to a Jeffcott rotor with a breathing crack. J. Sound Vib. **332**, 3881–3892 (2013)
19. Pilkey, W.D.: Analysis and Design of Elastic Beams: Computational Methods. Wiley, New York (2002)
20. Lalanne, M., Ferraris, G.: Rotordynamics Prediction in Engineering. Wiley, New York (1997)
21. Ishida, Y., Yamamoto, T.: Linear and Nonlinear Rotordynamics: A Modern Treatment with Applications. Wiley-VCH Verlag GmbH & Co. KGaA, Weinheim (2012)
22. Fung, T.C.: Unconditionally stable higher-order Newmark methods by sub-stepping procedure. Comput. Methods Appl. Mech. Eng. **147**, 61–84 (1997)
23. Zhang, L., Zu, J.W., Zheng, Z.: The stochastic Newmark algorithm for random analysis of multi-degree-of-freedom nonlinear systems. Comput. Struct. **70**, 557–568 (1999)
24. Chiba, F., Kako, T.: Newmark's method and discrete energy applied to resistive MHD equation. Vietnam J. Math. **30** (2002)
25. Gawronski, W.K.: Advanced Structural Dynamics and Active Control of Structures. Springer-Verlag, New York (2004)
26. Swanson, E., Powell, C.D., Weissman, S., Wasserman, A.: A practical review of rotating machinery critical speeds and modes. Sound Vib. **8** (2005)
27. AL-Shudeifat, M.A.: On the finite element modeling of the asymmetric cracked rotor. J. Sound Vib. **332**, 2795–2807 (2013)
28. Sawicki, J.T., Storozhev, D.L., Lekki, J.D.: Exploration of NDE properties of AMB supported rotors for structural damage detection. J. Eng. Gas Turbines Power **133**, 102501 (2011)
29. Penny, J.E., Friswell, M.I., Zhou, C.: Condition monitoring of rotating machinery using active magnetic bearings. In: ISMA 2006, pp. 3497–3506 (2006)
30. Sawicki, J.T.: Rotor crack detection using active magnetic bearings. Solid State Phenom. **144**, 9–15 (2009)